

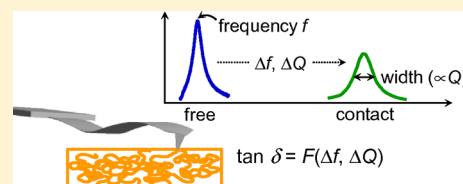
Measurement of Viscoelastic Loss Tangent with Contact Resonance Modes of Atomic Force Microscopy

Donna C. Hurley,^{*,†} Sara E. Campbell,^{†,||} Jason P. Killgore,^{†,‡} Lewis M. Cox,[‡] and Yifu Ding[‡]

[†]National Institute of Standards & Technology, Boulder, Colorado 80305, United States

[‡]Department of Mechanical Engineering, University of Colorado, Boulder, Colorado 80309, United States

ABSTRACT: We show how atomic force microscopy techniques based on contact resonance (CR) can be used to measure the viscoelastic loss tangent $\tan \delta$ of polymeric materials. The method does not require intermediate calculation of loss and storage moduli, calibration measurements, or use of the conventional CR tip shape parameter. We present the method's physical concepts and sensitivity calculations for typical experimental parameters. In addition, CR experiments were performed on four homogeneous polymer samples (polystyrene, high-density polyethylene, and two commercial photostress polymers) with $\tan \delta$ in the range from approximately 0.02 to 0.2. Results compare favorably to those obtained by microscale dynamic nanoindentation and macroscale dynamic mechanical analysis. These results show the potential of CR modes for nanoscale viscoelastic measurements of polymers and biomaterials.



INTRODUCTION

For successful development of new polymers and biomaterials, measurements of micro- and nanoscale mechanical properties are important to evaluate performance and reliability. Data of interest in such materials primarily concern viscoelastic quantities such as storage modulus E' , loss modulus E'' , loss tangent $\tan \delta$, and creep compliance. To meet these needs, a number of techniques based on atomic force microscopy (AFM) have been developed.^{1–7} In particular, we have previously demonstrated contact resonance (CR) modes of AFM for quantitative measurements of viscoelastic properties of polymers.^{8,9} A dynamic contact AFM mode, CR measures the frequency and quality factor of the cantilever's resonant peak while the tip is in contact with the sample. In our previous work, CR maps of *relative* E' and E'' were obtained for a binary polymer blend. The results were in good agreement with relative values obtained by dynamic mechanical analysis (DMA) on the bulk constituents. However, *absolute* values of E' and E'' were not determined. The reason was that standard CR approaches require calibration measurements on a material with known values of E' and E'' to determine absolute values. However, it is often challenging to obtain reliable values of such information, particularly for the loss modulus E'' .

To overcome these issues, we have devised a new viscoelastic CR method for direct determination of the absolute value of $\tan \delta$. Here, we present the method's physical principles and consider its theoretical sensitivity and applicability. We also assess its accuracy through measurements on several homogeneous polymeric materials. Results are compared with those obtained by more conventional techniques, namely DMA and dynamic nanoindentation (DNI). Through this evaluation, we find that CR is a highly promising AFM mode for quantitative characterization of viscoelastic materials on the nanoscale.

CONTACT RESONANCE THEORY FOR LOSS TANGENT

In simplest terms, viscoelastic CR^{9,10} involves measuring the contact resonance frequency f^{CR} and quality factor Q^{CR} at each image location. (For simplicity of notation, we drop the subscript n denoting the n th flexural resonance.) The resulting images of f^{CR} and Q^{CR} are then used to calculate maps of viscoelastic quantities such as storage modulus E' and loss modulus E'' . This analysis procedure has been described in detail elsewhere.^{8,10} Here, we only summarize the steps involved in the procedure.

First, an Euler–Bernoulli model for the dynamic motion of the cantilever in contact is used to determine properties of the tip–sample contact from f^{CR} and Q^{CR} . Knowledge of the frequency f^{free} and quality factor Q^{free} for the corresponding free vibrational mode is used to characterize the cantilever properties. The tip–sample contact is modeled as a Kelvin–Voigt element, namely, a linear elastic spring with spring constant k^* in parallel with a dashpot of damping σ . The small amplitude of the CR modulation (approximately tens of picometers) aids in modeling the contact as a linear interaction. Although a Kelvin–Voigt element oversimplifies the response of real polymeric materials, it is a useful starting point for technique development.

Analysis of f^{CR} and Q^{CR} with the beam dynamics model¹¹ yields the normalized contact stiffness $\alpha = k^*/k_L$ and contact damping $\beta = \sigma L_1 / (9EI\rho A)^{1/2}$. Here, $k_L = 3EI/L_1^3$ is the spring constant of the cantilever. L_1 is the position of the AFM tip along the cantilever's length L and is also expressed in terms of a relative tip position $\gamma = L_1/L$. The quantities E , I , ρ , and A are

Received: September 25, 2013

Revised: November 4, 2013

Published: November 26, 2013

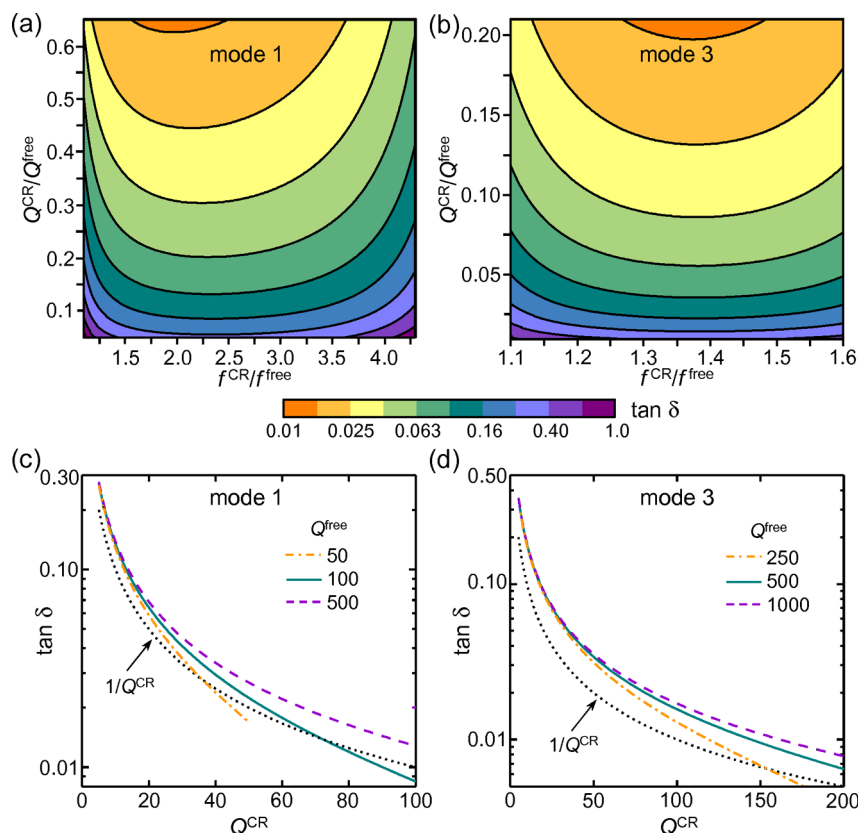


Figure 1. Viscoelastic loss tangent $\tan \delta$ calculated with eq 4. (a, b) Maps of $\tan \delta$ as a function of normalized cantilever frequency $f^{\text{CR}}/f^{\text{free}}$ and quality factor $Q^{\text{CR}}/Q^{\text{free}}$ for the first and third flexural eigenmodes, respectively. $Q^{\text{free}} = 100$ was used in (a) and $Q^{\text{free}} = 500$ was used in (b). (c, d) Dependence of $\tan \delta$ on Q^{CR} for the first and third modes, respectively. In (c), $f^{\text{CR}}/f^{\text{free}} = 2.55$ and $Q^{\text{free}} = 50, 100,$ and 200 were used, while $f^{\text{CR}}/f^{\text{free}} = 1.35$ and $Q^{\text{free}} = 250, 500,$ and 1000 were used in (d). Dotted lines indicate $1/Q^{\text{CR}}$ behavior. Note the logarithmic scales. All results were calculated with relative tip position $\gamma = 0.96$.

the Young's modulus, area moment of inertia, density, and cross-sectional area, respectively, of the idealized rectangular cantilever beam.

Given α and β , viscoelastic quantities such as E' and E'' are then determined by use of a contact mechanics model. Typically, Hertzian contact (i.e., no adhesion) is assumed. Calibration data, for instance through complementary measurements, are required to obtain absolute values of E' and E'' . Interpretation also requires assumptions about the tip shape; often, the solutions for a hemispherical tip and a flat punch are used as upper and lower bounds. As mentioned above, we previously applied this approach to a polypropylene–polystyrene blend and achieved good agreement with DMA data.⁸

Here we consider an expression for the viscoelastic loss tangent $\tan \delta = E''/E'$. However, our expression is derived directly from the cantilever beam dynamics model and does not involve intermediate calculation of E'' and E' . It originates from the relation^{12,13}

$$\tan \delta = \frac{2\pi f^{\text{CR}} \sigma}{k^*} \quad (1)$$

Equation 1 can be expressed in terms of α and β by use of the relations given above for k^* , σ , and k_L . We also use¹⁴

$$2\pi f^{\text{CR}} = (yL)^2 \sqrt{\frac{EI}{\rho AL^4}} \quad (2)$$

where the normalized contact wavenumber yL for a given flexural eigenmode is related to the corresponding normalized free wavenumber xL through

$$(yL)^2 = (xL)^2 \frac{f^{\text{CR}}}{f^{\text{free}}} \quad (3)$$

xL is the corresponding solution to the characteristic equation for free flexural vibration: $1 + \cos(xL) \cosh(xL) = 0$, with $xL = [1.8751, 4.6941, 7.8548]$ for flexural mode $n = [1, 2, 3]$. Substituting all of these relations into eq 1, we obtain

$$\tan \delta = \frac{(xL)^2 \gamma^2 \beta f^{\text{CR}}}{\alpha f^{\text{free}}} \quad (4)$$

Equation 4 is a slightly modified form of one published previously without derivation.¹⁵ It now includes a γ^2 term that was previously omitted.

Use of eq 4 to determine viscoelastic properties is attractive for several reasons. Unlike existing contact resonance methods to determine E' and E'' , this approach does not involve calibration data or comparison measurements on a material with known properties. This is noteworthy because uncertainty remains regarding the accurate comparison of viscoelastic data from different measurement methods. If desired, measurements of $\tan \delta$ with eq 4 could be combined with absolute measurements of storage modulus E' to yield a complete set of property data. Also of note is the fact that eq 4 does not require detailed information about the tip–sample contact area

such as tip geometry, applied force, or tip–sample creep. “Tip geometry” refers to the use of a parameter m to characterize the shape of the axisymmetric indenter tip. General elastic contact mechanics allow calculation of modulus values with m , which typically ranges from $m = 1$ for a flat punch to $m = 3/2$ for a hemisphere. CR experiments often report results with these two m values as the range of possible values. The absence of a tip shape parameter in eq 4 thus improves measurement precision without specifying m . Concerning creep, measurements can be made either immediately after initial tip–sample contact or after waiting for tip–sample creep to mostly equilibrate. In either case, the data acquisition rate for a CR spectrum at a single position should be much faster than the characteristic time scale for creep. Finally, the method does not require calibration of the cantilever spring constant k_L .

It should be noted that the derivation of eq 4 involves some assumptions. First, our current model^{9,10} leads to a relatively simple, closed-form expression for α and β with the assumption $a \gg b$, where $(a + ib) = \gamma L$ is the normalized wavenumber. The assumption $a \gg b$ sets a lower limit on the value of Q^{CR} for which our model is valid due to the relation¹⁰ $1/Q^{\text{CR}} \approx 1/Q_{\text{sample}} = 4b/a$. Thus, for $b/a \leq 0.05$, it is necessary that $Q^{\text{CR}} \geq 5$. (For comparison, Q^{CR} in this study ranged from approximately 15 to 80 depending on sample.) Second, it is important to remember that contact resonance methods measure the tip–sample interaction. It is typically assumed that dissipation in the measurement corresponds entirely to the properties of the sample, which may or may not be the case. For instance, energy dissipation due to a surface water layer will contribute to the measured damping and lead to higher apparent values of $\tan \delta$. Also, in some experimental conditions, squeeze-film damping and other hydrodynamic effects will affect damping.¹⁶ Finally, the internal damping of the tip is considered negligible (i.e., $Q_{\text{tip}} \gg Q_{\text{sample}}$ or $E''_{\text{tip}} \approx 0$). This assumption is valid for measurements with a silicon cantilever tip on materials such as the polymers used here. However, it will break down for measurements involving materials with extremely low loss tangent (e.g., thin metallic films,¹⁷ metallic glasses¹⁸).

Equation 4 can be better understood with contour plots and graphs such as those shown in Figure 1. The plots in Figures 1a and 1b show the values of $\tan \delta$ calculated with eq 4 as a function of normalized frequency $f^{\text{CR}}/f^{\text{free}}$ and normalized quality factor $Q^{\text{CR}}/Q^{\text{free}}$ for the first ($n = 1$) and third ($n = 3$) flexural modes, respectively. The plots were calculated assuming $Q^{\text{free}} = 100$ for mode 1 and $Q^{\text{free}} = 500$ for mode 3, consistent with typical experimental values. Corresponding plots for other values of Q^{free} , as well as those for the second flexural mode, show qualitatively similar behavior. For both plots, the minimum value of $f^{\text{CR}}/f^{\text{free}}$ (x -axis) was set to 1.1, while its maximum value was chosen based on the theoretical limit for a clamped-pinned cantilever of mode n : $f^{\text{CR}}/f^{\text{free}} = [4.39, 2.26, 1.69]$ for $n = [1, 2, 3]$. The minimum value of $Q^{\text{CR}}/Q^{\text{free}}$ (y -axis) was set based on Q^{free} and the condition $Q^{\text{CR}}/Q^{\text{free}} \geq 5$ discussed above. The maximum value of $Q^{\text{CR}}/Q^{\text{free}}$ was chosen such that the plot included a region with $\tan \delta \approx 0.01$.

Inspection of Figures 1a and 1b reveals that although $\tan \delta$ is inversely related to Q^{CR} , the exact relation depends on the value of $f^{\text{CR}}/f^{\text{free}}$. This is because the contact stiffness α and contact damping β in eq 4 depend on both f^{CR} and Q^{CR} .¹⁰ As a result, for a fixed value of $Q^{\text{CR}}/Q^{\text{free}}$ (constant γ) the value of $\tan \delta$ varies depending on $f^{\text{CR}}/f^{\text{free}}$ (x). The variation is more significant as the lower and upper limits of $f^{\text{CR}}/f^{\text{free}}$ are

approached. A practical implication of this behavior involves multicomponent materials that exhibit a range of f^{CR} . In such cases, it can be misleading to evaluate $\tan \delta$ or relative damping solely on Q^{CR} .

Additional insight can be gained from Figures 1c and 1d, which plot $\tan \delta$ as a function of Q^{CR} for fixed values of $f^{\text{CR}}/f^{\text{free}}$. The values of $f^{\text{CR}}/f^{\text{free}}$ used to generate Figures 1c and 1d lie approximately in the middle columns of Figures 1a and 1b, respectively. In each plot, the solid, dashed, and dash-dotted (colored) curves correspond to three different values of Q^{free} . For comparison, the dotted black lines show a $1/Q^{\text{CR}}$ behavior. The graphs show that for constant $f^{\text{CR}}/f^{\text{free}}$ the relation¹⁷ $\tan \delta \approx 1/Q^{\text{CR}}$ is qualitatively reasonable, especially for higher values of Q^{free} . However, the relation is a poor estimate of the absolute value of $\tan \delta$ and generally underestimates $\tan \delta$ significantly. For instance, due to the limit $Q^{\text{CR}} \geq 5$ imposed in our model, the maximum possible value of $1/Q^{\text{CR}}$ is 0.2, whereas eq 4 yields maximum values of $\tan \delta$ of approximately 0.3–0.4 depending on the choice of mode and Q^{free} . Moreover, the magnitude of the discrepancy depends on mode, with larger differences for mode 3 than for mode 1.

Figure 1 also provides insight into the capabilities and limits of current contact resonance methods for viscoelastic measurements. The plots show that precise and accurate measurements of $\tan \delta$ require sensitive and accurate determination of Q^{CR} , particularly for large $\tan \delta$ (~ 0.3 or greater). Revision of the analysis model to modify the approximation mentioned above or careful choice of experimental parameters such as mode n , Q^{free} , and $f^{\text{CR}}/f^{\text{free}}$ may enable measurements over a wider range of loss tangent values.

MATERIALS AND METHODS

Materials. Samples were cut from four types of polymer sheet stock. In selecting the materials, we restricted candidates to commercially available,¹⁹ relatively stiff polymers (those with E' from approximately 1 to 4 GPa). Based on reported values in the literature, the materials were expected to span a range of $\tan \delta$ from approximately 0.01 to 0.2. Two samples consisted of polystyrene (PS, #ST313120, Goodfellow USA) and high-density polyethylene (HDPE, #ET323100, Goodfellow USA). The remaining two samples were photoelastic coating materials (PhotoStress PS-1 and PS-3, Vishay Precision Group). To avoid confusion with polystyrene, these materials are denoted here as V-1 and V-3, respectively. The chemical composition of these materials was not provided by the manufacturer, but they were chosen due to their prior use in the instrumented indentation (nanoindentation) community for viscoelastic studies.^{20,21} As a rough guide, Table 1 shows literature values reported for E' and $\tan \delta$ in our materials. For the PS and HDPE samples, the polymer type does not uniquely identify the chemical composition due to potential differences in molecular weight and polydispersity. Thus, the values in Table 1 for PS and HDPE should not be considered

Table 1. Representative Literature Values for Storage Modulus E' and Loss Tangent $\tan \delta$ for Polystyrene (PS), High-Density Polyethylene (HDPE), and Photoelastic Coating Materials V-1 and V-3^a

material	E' (GPa)	$\tan \delta$	ref(s)
PS	2.8–2.9	0.015–0.025	22, 23
V-1	2.1–2.6	0.01–0.08	20
HDPE	0.9–2.1	0.06–0.15	24–26
V-3	1.1–1.4	0.150–0.175	20

^aData shown represent measurements at room temperature (approximately 20–25 °C) and low frequencies (1–75 Hz).

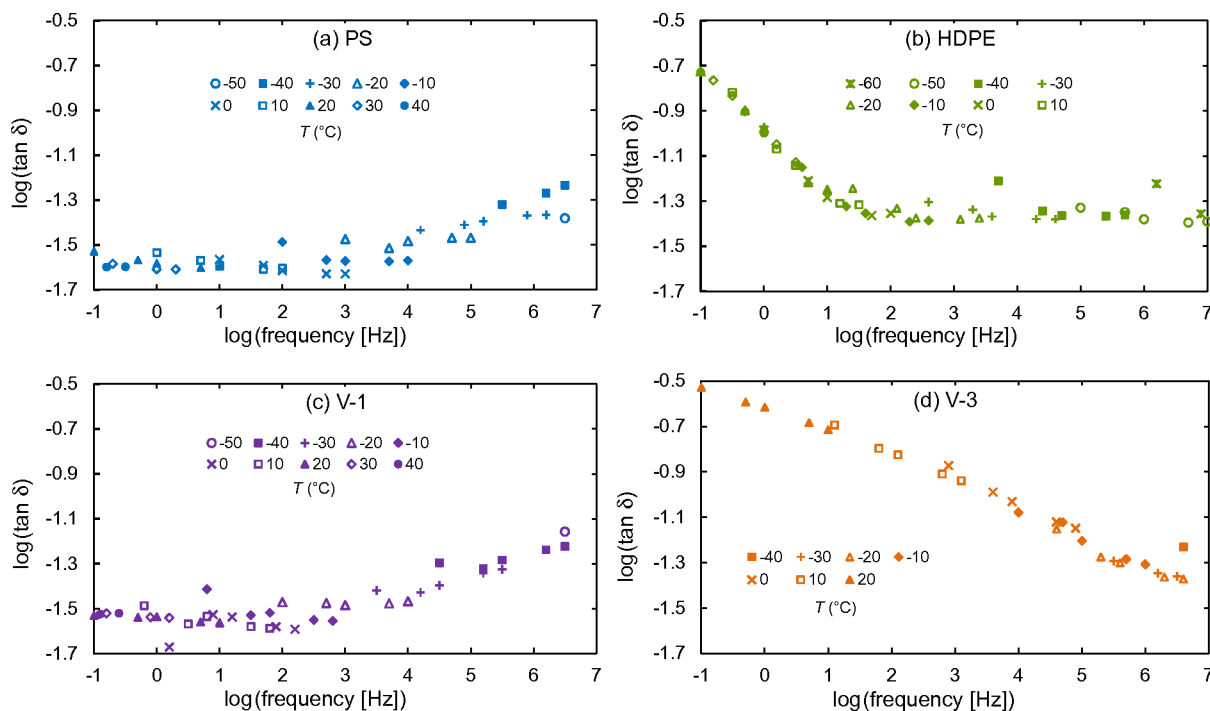


Figure 2. Values of $\tan \delta$ obtained with time–temperature superposition analysis of DMA data for the (a) PS, (b) V-1, (c) HDPE, and (d) V-3 specimens. The symbols indicate the temperature at which each data set was acquired. The reference temperature used to shift all data sets was 20 °C.

definitive. However, our V-1 and V-3 samples originated from the same source as in other studies. Therefore, it is likely that their composition is virtually identical to that utilized in earlier studies, and comparison of results is more valid.

Sample surfaces were prepared by ultramicrotomy with a diamond blade at room temperature. Surface smoothness was found to be a key factor in obtaining reliable results that minimized data scatter. Through much experimentation, ultramicrotomy emerged as the best method of surface preparation available to us. For instance, the relative data scatter in $\tan \delta$ (defined as one measurement standard deviation divided by the average) was 29%–55% on the as-received surfaces, while it ranged from 4% to 19% after ultramicrotome preparation. For the ultramicrotomed surfaces, the RMS roughness determined by tapping-mode topography imaging was 20 nm or less for $2 \mu\text{m} \times 2 \mu\text{m}$ regions.

CR Methods. All contact resonance data were acquired with a single cantilever. The nominal properties of the cantilever provided by the manufacturer are spring constant $k_L = 1.0 \text{ N/m}$, length $224 \mu\text{m}$, width $25 \mu\text{m}$, and thickness $2.3 \mu\text{m}$. The natural frequency of the cantilever's lowest flexural mode was $56.02 \pm 0.02 \text{ kHz}$. All experiments were performed with a set point voltage of 0.4 V. With the measured cantilever sensitivity of 170.4 nm/V , this corresponds to a cantilever deflection $d = 68 \text{ nm}$. Therefore, the static applied force F during the measurements as determined by $F = k_L d$ was estimated to be approximately 70 nN. With this force, Hertzian contact mechanics predicts a maximum stress directly beneath the tip of hundreds of megapascals, which is several times larger than the yield strength of typical stiff polymers. Although the stress amplitude falls off rapidly from this maximum in all directions, some plastic deformation within the contact region is likely. However, dynamic nanoindentation methods^{12,13,27,28} provide evidence that a material's viscoelastic response can be probed by elastic–plastic deformation. Operation in a purely elastic deformation regime may be possible through use of AFM tips with larger radius of curvature and/or through smaller applied forces.^{4,29,30}

CR experiments were performed with a commercial AFM instrument (MFP-3D, Asylum Research/Oxford Instruments) that has a built-in capability for acquisition of contact resonance spectra.

Cantilever excitation in the CR frequency range (approximately 1.1–1.3 MHz) was achieved by use of a nonstandard cantilever holder with a high-frequency, heavily damped piezoelectric chip (AM-FM holder, Asylum Research/Oxford Instruments). Measurements were performed at the ambient temperature of the AFM acoustic isolation chamber. Prior to data acquisition, the interior of the AFM acoustic isolation hood was flooded with compressed dry air until the relative humidity in the chamber was 5% or less. This procedure was intended to minimize formation of water layers on the samples. To minimize acoustic noise and turbulent forces during data acquisition, air flow was stopped immediately before data acquisition.

Measurements were performed with the cantilever's third flexural eigenmode, which had a free frequency $f^{\text{free}} = 1004.0 \pm 0.04 \text{ kHz}$ and free quality factor $Q^{\text{free}} = 543 \pm 2$. Use of the third mode ensured good measurement sensitivity and minimized the effect of lateral tip–sample interactions.³⁰ In the experiments, CR frequency and quality factor maps were obtained with a user-written subroutine within the AFM software. The subroutine consisted of the following steps: (1) move the cantilever to the next sample position, (2) engage the tip with the surface at the chosen set point voltage relative to the free deflection, (3) acquire a CR spectrum over the selected frequency range, (4) retract the tip out of contact, and (5) fit the data to a damped harmonic oscillator function and record the resulting values of f^{CR} and Q^{CR} . The entire process was repeated at each position in the image grid.

Following this procedure, arrays of 10×10 pixels were acquired on each of the four samples in succession. The entire process was performed three times, with the sample order changed randomly each time. Thus, the CR values reported below represent the average and standard deviation of 300 points. A relatively short acquisition period (0.2 s per spectrum) was chosen to minimize creep during the measurement. Immediately before each map was acquired, individual CR spectra were obtained for the second and third flexural modes. These point measurements were used to determine the relative tip position γ from the mode-crossing method.¹⁴ The value of the relative tip position γ obtained, which ranged from approximately 0.95 to 0.97 in these experiments, was then used in the analysis of the entire image.

DMA Methods. In dynamic mechanical analysis (DMA), a sinusoidal deformation is applied to the specimen at a specified frequency and temperature. The resulting stress that accompanies this deformation is recorded. The obtained stress, strain, and phase difference between them are measured and used to determine the storage modulus E' and the loss modulus E'' of the specimen. Furthermore, the internal loss $\tan \delta = E''/E'$ can be determined. Both temperature and oscillation frequency can be systematically varied to provide a “spectrum” of the mechanical properties. The results reported here were obtained with a commercial DMA instrument (DMA Q800, TA Instruments) with a film-tension clamping geometry. Specimens approximately 1 mm thick, 5 mm wide, and 10–18 mm long were cut from the same polymer sheets used in the AFM experiments. Measurements were performed at temperatures from -100 to 40 °C in 10 °C increments. At each temperature, measurements were made at 0.1, 0.5, 1, 5, and 10 Hz. Measurements were performed with a controlled strain amplitude of 0.01%. The resulting oscillation amplitude during the experiments was approximately 1 μm , and the strain rate (product of strain and oscillation frequency) ranged from approximately 10^{-3} to 10^{-5} s^{-1} .

Time–temperature superposition³¹ (TTS) was employed to generate master curves with a reference temperature of 20 °C. The corresponding shift factors for PS, HDPE, and V-1 were observed to follow an Arrhenius-type temperature dependence, indicated by the linear trends in Figure 2. This dependence is consistent with previous work investigating secondary relaxations of polymers in the glassy state.³² The shift factors for the V-3 material also demonstrate Arrhenius-type behavior at lower temperatures; however, a nonlinear tail was observed for temperatures above 0 °C, which corresponds to the α relaxation in this material with relatively low glass transition temperature. The activation energies associated with the Arrhenius-type behavior were determined by plotting the shift factors as an inverse function of temperature. The resulting values for the activation energy of PS, HDPE, V-1, and V-3 were 148, 105, 118, and 130 kJ/mol, respectively. The TTS master curves serve to forecast the frequency dependence of $\tan \delta$ across frequencies not directly accessible by the DMA instrument.

DNI Methods. In dynamic nanoindentation (DNI),^{12,13,27,28} the standard instrumented indentation (also called nanoindentation) technique is modified by superposition of a low-amplitude, sinusoidal load on the quasi-static load. Lock-in detection methods are used to obtain the amplitude and phase shift of the material response at the ac frequency. The response is modeled with a Kelvin–Voigt element to determine the storage modulus E' , loss modulus E'' , and loss tangent $\tan \delta = E''/E'$ versus oscillation frequency. The results reported here were obtained with a commercial DNI instrument (Triboindenter TI-900, Hysitron) with use of a diamond Berkovich indenter tip. Specimens were cut from the same polymer sheets used in the AFM experiments.

In each measurement trial, the following sequence of steps was performed: (1) engage tip to surface, (2) perform force ramp from zero to maximum (~ 1.7 mN in 30 s), (3) hold at maximum load to minimize the contribution of creep to data acquisition (120 s), (4) acquire data at constant ac load (20 μN with the aforementioned 1.7 mN dc offset), and (5) perform force unload ramp (30 s). During data acquisition, the oscillation frequency was increased from 10 to 300 Hz and then decreased back to 10 Hz with a hold for 100 cycles at each oscillation frequency. A total of nine measurement trials were performed on each sample, ultimately resulting in 18 values of $\tan \delta$ for each sample at each frequency. The results discussed below and in Figure 3 represent the average and one standard deviation of the individual measurements.

RESULTS AND DISCUSSION

DMA Results. The values for $\tan \delta$ obtained by TTS analysis of the DMA data are shown in Figures 2a–d for PS, HDPE, V-1, and V-3, respectively. Comparison of the individual graphs reveals that the different materials exhibit different frequency responses. For HDPE in Figure 2b, $\tan \delta$

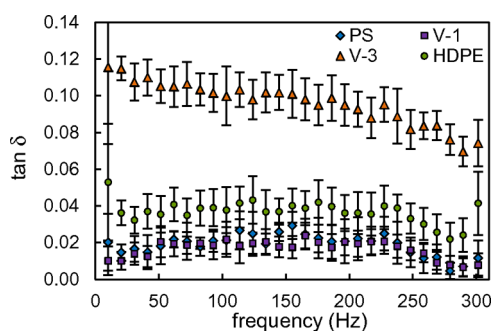


Figure 3. Values of $\tan \delta$ obtained with dynamic nanoindentation on the PS, HDPE, V-1, and V-3 specimens.

remains almost constant above ~ 100 Hz. The flatness of its frequency response means that this material might be useful for screening viscoelastic techniques because any method should yield nearly the same value of $\tan \delta$ regardless of its characteristic frequency. In contrast, Figure 2d shows that $\log(\tan \delta)$ for V-3 is a linear function of $\log(\text{frequency})$ over at least 6 decades (approximately 0.1 Hz–100 kHz). This sensitivity to frequency might also be useful for assessing new measurement techniques. The plots of $\tan \delta$ for PS and V-1 in Figures 2a and 2c, respectively, show qualitatively different frequency behavior to the plots for HDPE and V-3 in Figures 2b and 2d. For both PS and V-1, $\tan \delta$ is relatively constant with frequency below ~ 1 kHz and increases monotonically at higher frequencies. In Figure 2a, the slight increase in $\tan \delta$ with higher frequencies is consistent with a previously observed secondary relaxation in PS at lower temperatures.³³

To summarize the DMA results for comparison with the DNI and CR data, we report two values of $\tan \delta$ for each material. The first represents a low-frequency result and is the single value of $\tan \delta$ measured at 10 Hz and 20 °C (“DMA” in Figure 4). The second value corresponds to the results obtained

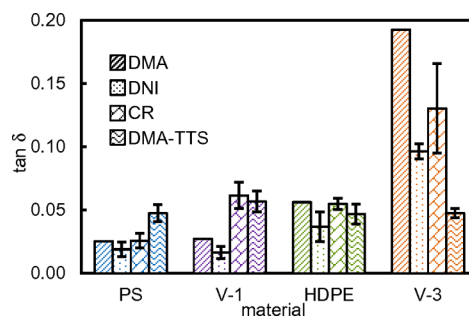


Figure 4. Summary of experimental results. “DMA” represents single measurements acquired at 10 Hz and 20 °C. “DMA-TTS” represents average values at ~ 1 MHz through TTS analysis of DMA data. “DNI” indicates values averaged from 10 to 300 Hz. “CR” values are averages of data at ~ 1.2 MHz.

with use of TTS principles for frequencies similar to those used in the contact resonance measurements. It is the average and one standard deviation of four to six TTS values within ± 0.5 decade of 1 MHz (i.e., approximately 300 kHz–3 MHz). These values are denoted as “DMA-TTS” in Figure 4.

DNI Results. The DNI results for $\tan \delta$ are shown in Figure 3 for all four materials. Consistent with our DMA-TTS data, the V-3 results show a clear decrease with frequency. Results for the other three materials are relatively flat with frequency,

which is also consistent with our DMA-TTS results in this frequency range. In terms of absolute $\tan \delta$, the values for PS and V-1 are the lowest overall and very similar. The values for HDPE are slightly higher, while those for V-3 are distinctly the largest of all materials. The slight bow versus frequency in the plots suggests that the dynamic calibration procedure to correct for system resonances was not completely effective. To minimize the impact of this effect on the reported DNI values of $\tan \delta$, we report the average and one standard deviation of $\tan \delta$ across the entire frequency range from 10 to 300 Hz. Although this approach ignores any strong frequency dependence of $\tan \delta$ (such as that seen for V-3), it provides overall “low-frequency” values with which to summarize the DNI results.

CR Results. The bar chart in Figure 4 summarizes our experimental results. We are encouraged to observe that the absolute values of $\tan \delta$ obtained with CR techniques are consistent overall with both the literature values in Table 1 and our other experimental results. In fact, the values are not only same order of magnitude but within a factor of 2 or 3. This observation is true for values from about 0.02 to 0.2, that is, approximately 1 order of magnitude in $\tan \delta$.

Closer scrutiny of Figure 4 allows insight into the relative agreement of $\tan \delta$ values for the same material obtained by different methods. For the V-1 and HDPE samples, there is very good agreement between the CR results and those obtained at similarly high frequencies (DMA-TTS). Such agreement based on direct frequency comparison is consistent with our previous results on CR measurement of loss and storage moduli.⁸ Note that all techniques yielded very similar values of $\tan \delta$ for HDPE. This behavior is consistent with the virtually flat response of $\tan \delta$ for HDPE with frequency shown in Figure 2b. These results emphasize the value of identifying additional “constant loss” materials that span a wide range of $\tan \delta$.

The picture is less clear for the V-3 and PS samples. The CR results are the correct absolute value but show relatively poor agreement with the high-frequency DMA-TTS results. Several issues can be identified as possible contributors to this complex picture. For instance, there is debate on the accuracy or repeatability of absolute values obtained by DMA-TTS, although the qualitative frequency dependence is generally considered reliable. Another issue is the fact that each technique probes a different length scale. Therefore, micro- and nanoscale material inhomogeneity could skew the results. Previous comparisons of measurements at different length scales revealed similar discrepancies, even at same frequency.²⁰ The strong frequency dependence of $\tan \delta$ in V-3, shown in Figure 2d, may be a contributing factor in this regard. Most importantly, each technique involves substantially different values of strain and strain rate. The strain rate depends not only on frequency but also on oscillation amplitude, which is roughly a few micrometers for DMA, a few nanometers for DNI, and perhaps tens of picometers for CR. Also, due to the force dependence of contact area arising from nonflat tips, the strain rate in DNI and CR varies throughout each ac oscillation. Interpretation is further complicated by the fact that DMA methods represent a one-dimensional strain geometry, while DNI and CR are three-dimensional.

For these reasons, we believe that further detailed analysis of Figure 4 is not useful at this point. We instead view the overall agreement within a factor of 2–3 between the CR and other results as highly promising. Further development and validation

of the CR method—or indeed any micro- or nanoscale method—will require careful consideration of these and similar issues.

Future investigation in several areas could strengthen and refine the results of this initial work. The measurements here were performed in point spectroscopy mode with a stationary tip. Extension to 2D imaging with either CR point map^{8,34} or scanning techniques^{35,36} is straightforward. The introduction of more complex models for the tip–sample contact in CR (e.g., standard linear solid, Prony series, fractional calculus/elements) should also be pursued. Finally, improvements in understanding, measuring, and controlling strain and strain rate would be valuable not just for CR but many other AFM modes. This might be achieved, for instance, with use of magnetic,³⁷ interferometric,³⁸ or electron microscopy³⁹ approaches to apply or monitor forces and deformation.

SUMMARY AND CONCLUSIONS

We have presented a contact-resonance-based AFM method to measure absolute values of nanoscale viscoelastic loss tangent $\tan \delta$. With this approach, $\tan \delta$ is determined from the frequency and quality factor of the cantilever's resonant peak without intermediate calculation of loss modulus and storage modulus. The method requires no calibration measurements and no CR tip shape parameter. Measurements were performed on several polymer samples with loss tangent values that spanned an order of magnitude (~ 0.02 – 0.2). Experimental CR results for $\tan \delta$ were very similar to results obtained with microscale (dynamic nanoindentation) and macroscale (dynamic mechanical analysis) techniques. Further work is needed to fully characterize the three-dimensional strain and strain rates that are present in contact AFM methods such as CR. Such insight will enable better comparison of CR results to data obtained by techniques that probe larger length scales and at different measurement frequencies. Nonetheless, our results demonstrate advanced measurement capabilities that will prove valuable in the successful development of micro- and nanoscale polymers and biomaterials.

AUTHOR INFORMATION

Corresponding Author

*E-mail: donna.hurley@nist.gov (D.C.H.).

Present Address

||S.E.C.: Covidien, Boulder, CO 80301.

Notes

The authors declare no competing financial interest.

ACKNOWLEDGMENTS

We thank Bryon Donohoe (National Renewable Energy Laboratory) for assistance with sample preparation by ultramicrotomy and Chris Poling (NIST) for assistance with the dynamic nanoindentation measurements. We thank Ryan Tung (NIST) for correcting the expression for $\tan \delta$ and for other productive discussions. We value discussions with Robert Cook (NIST), Nigel Jennett (National Physical Laboratory, UK), and Michelle Oyen (Cambridge University, UK). This work was performed while SEC held a National Research Council Associateship Award at NIST. L.M.C. and Y.D. acknowledge funding support from the National Science Foundation under Grant CMMI-1233626.

■ REFERENCES

- (1) Kajiyama, T.; Tanaka, K.; Ohki, I.; Ge, S.-R.; Yoon, J.-S.; Takahara, A. *Macromolecules* **1994**, *27*, 7932–7934.
- (2) Chizhik, S. A.; Huang, Z.; Gorbunov, V. V.; Myshkin, N. K.; Tsukruk, V. V. *Langmuir* **1998**, *14*, 2606–2609.
- (3) Attard, P. J. *Phys.: Condens. Matter* **2007**, *19*, 473201.
- (4) Moeller, G. J. *Polym. Sci., Part B: Polym. Phys.* **2009**, *47*, 1573–1587.
- (5) McConney, M. E.; Singamaneni, S.; Tsukruk, V. V. *Polym. Rev.* **2010**, *50*, 235–286.
- (6) Raman, A.; Trigueros, S.; Cartagena, A.; Stevenson, A. P. Z.; Susilo, M.; Nauman, E.; Antoranz Contera, S. *Nat. Nanotechnol.* **2011**, *6*, 809–814.
- (7) Garcia, R.; Proksch, R. *Eur. Polym. J.* **2013**, *49*, 1897–1906.
- (8) Killgore, J. P.; Yablon, D. G.; Tsou, A. H.; Gannepalli, A.; Yuya, P. A.; Turner, J. A.; Proksch, R.; Hurley, D. C. *Langmuir* **2011**, *27*, 13983–13987.
- (9) Yuya, P. A.; Hurley, D. C.; Turner, J. A. *J. Appl. Phys.* **2008**, *104*, 074916.
- (10) Yuya, P. A.; Hurley, D. C.; Turner, J. A. *J. Appl. Phys.* **2011**, *109*, 113528.
- (11) Rabe, U.; Turner, J.; Arnold, W. *Appl. Phys. A: Mater. Sci. Process.* **1998**, *66*, S277–S282.
- (12) Loubet, J. L.; Oliver, W. C.; Lucas, B. N. *J. Mater. Res.* **2000**, *15*, 1195–1198.
- (13) Syed Asif, S. A.; Wahl, K. J.; Colton, R. J. *Rev. Sci. Instrum.* **1999**, *70*, 2408–2413.
- (14) Rabe, U.; Amelio, S.; Kester, E.; Scherer, V.; Hirsekorn, S.; Arnold, W. *Ultrasonics* **2000**, *38*, 430–437.
- (15) Campbell, S. E.; Ferguson, V. L.; Hurley, D. C. *Acta Biomater.* **2012**, *8*, 4389–4396.
- (16) Tung, R. C.; Killgore, J. P.; Hurley, D. C. *Rev. Sci. Instrum.* **2013**, *84*, 073703.
- (17) Caron, A.; Arnold, W. *Acta Mater.* **2009**, *57*, 4353–4363.
- (18) Wagner, H.; Bedorf, D.; Kuechemann, S.; Schwabe, M.; Zhang, B.; Arnold, W.; Samwer, K. *Nat. Mater.* **2011**, *10*, 439–442.
- (19) Certain commercial equipment, instruments, or materials are identified in this paper in order to specify the experimental procedure adequately. Such identification does not imply recommendation or endorsement by NIST, nor does it imply that the materials or equipment identified are necessarily the best available for the purpose.
- (20) Monclus, M. A.; Jennett, N. M. *Philos. Mag.* **2010**, *91*, 1308–1328.
- (21) Oyen, M. L. *Acta Mater.* **2007**, *55*, 3633–3639.
- (22) Araki, O.; Shimamoto, T.; Yamamoto, T.; Masuda, T. *Polymer* **2001**, *42*, 4433–4437.
- (23) Patra, N.; Salerno, M.; Diaspro, A.; Athanassiou, A. *Microelectron. Eng.* **2011**, *88*, 1849–1851.
- (24) Odegard, G. M.; Gates, T. S.; Herring, H. M. *Exp. Mech.* **2005**, *45*, 130–136.
- (25) Joshi, M.; Butola, B. S.; Simon, G.; Kukaleva, N. *Macromolecules* **2006**, *39*, 1839–1849.
- (26) Mohanty, S.; Verma, S. K.; Nayak, S. K. *Compos. Sci. Technol.* **2006**, *66*, 538–547.
- (27) Oliver, W. C.; Pharr, G. M. *J. Mater. Res.* **2004**, *19*, 3–20.
- (28) Syed Asif, S. A.; Wahl, K. J.; Colton, R. J.; Warren, O. L. *J. Appl. Phys.* **2001**, *90*, 1192–1200.
- (29) Dokukin, M. E.; Sokolov, I. *Macromolecules* **2012**, *45*, 4277–4288.
- (30) Killgore, J. P.; Hurley, D. C. *Nanotechnology* **2012**, *23*, 055702.
- (31) Ferry, J. D. *Viscoelastic Properties of Polymers*; Wiley: New York, 1980.
- (32) O’Connell, P. A.; McKenna, G. B. *J. Chem. Phys.* **1999**, *110*, 11054–11060.
- (33) Struik, L. C. E. *Polymer* **1987**, *28*, 57–68.
- (34) Jesse, S.; Kalinin, S. V.; Proksch, R.; Baddorf, A. P.; Rodriguez, B. J. *Nanotechnology* **2007**, *18*, 435503.
- (35) Gannepalli, A.; Yablon, D. G.; Tsou, A. H.; Proksch, R. *Nanotechnology* **2011**, *22*, 355705.
- (36) Kos, A. B.; Hurley, D. C. *Meas. Sci. Technol.* **2008**, *19*, 015504.
- (37) Jarvis, S. P.; Oral, A.; Weihs, T. P.; Pethica, J. B. *Rev. Sci. Instrum.* **1993**, *64*, 3515–3520.
- (38) Rugar, D.; Mamin, H. J.; Guethner, P. *Appl. Phys. Lett.* **1989**, *55*, 2588–2590.
- (39) Joachimsthaler, I.; Heiderhoff, R.; Balk, L. J. *Meas. Sci. Technol.* **2003**, *14*, 87–96.